University of Birmingham
Research at Birmingham

# Microstructure, Hardening, and Mechanical Properties of Hypoeutectic Al–Ce–Ni Alloys with Zr and Zr + Sc Additions and the Effect of Ultrasonic Melt Processing

Chankitmunkong, Suwaree; Wang, Feng; Limmaneevichitr, Chaowalit; Eskin, Dmitry G.

*DOI:*
10.1002/adem.202301045

*License:*
Creative Commons: Attribution (CC BY)

*Document Version*
Publisher's PDF, also known as Version of record

*Citation for published version (Harvard):*
Chankitmunkong, S, Wang, F, Limmaneevichitr, C & Eskin, DG 2023, 'Microstructure, Hardening, and Mechanical Properties of Hypoeutectic Al–Ce–Ni Alloys with Zr and Zr + Sc Additions and the Effect of Ultrasonic Melt Processing', *Advanced Engineering Materials*. https://doi.org/10.1002/adem.202301045

Link to publication on Research at Birmingham portal

**General rights**
Unless a licence is specified above, all rights (including copyright and moral rights) in this document are retained by the authors and/or the copyright holders. The express permission of the copyright holder must be obtained for any use of this material other than for purposes permitted by law.

•Users may freely distribute the URL that is used to identify this publication.
•Users may download and/or print one copy of the publication from the University of Birmingham research portal for the purpose of private study or non-commercial research.
•User may use extracts from the document in line with the concept of ‘fair dealing’ under the Copyright, Designs and Patents Act 1988 (?)
•Users may not further distribute the material nor use it for the purposes of commercial gain.

Where a licence is displayed above, please note the terms and conditions of the licence govern your use of this document.

When citing, please reference the published version.

**Take down policy**
While the University of Birmingham exercises care and attention in making items available there are rare occasions when an item has been uploaded in error or has been deemed to be commercially or otherwise sensitive.

If you believe that this is the case for this document, please contact UBIRA@lists.bham.ac.uk providing details and we will remove access to the work immediately and investigate.

Download date: 23. Sep. 2023

ADVANCED ENGINEERING MATERIALS
www.aem-journal.com

# Microstructure, Hardening, and Mechanical Properties of Hypoeutectic Al–Ce–Ni Alloys with Zr and Zr + Sc Additions and the Effect of Ultrasonic Melt Processing

*Suwaree Chankitmunkong, Feng Wang, Chaowalit Limmaneevichitr, and Dmitry G. Eskin**

**Ternary Al–Ce–Ni alloys have a potential in the manufacture of automotive and airspace components, as well as in replacing traditional aluminum alloys in high-temperature applications, which is determined by the formation of fine and thermally stable $Al_{11}Ce_3$ and $Al_3Ni$ eutectic. Herein, the microstructure and mechanical properties of a hypoeutectic $Al_4Ce_2Ni$ alloy using Zr and Zr + Sc additions combined with ultrasonic melt processing and dispersion hardening are improved. As a result, the grain structure of the as-cast alloys is significantly refined and the annealing at 350 °C leads to a considerable hardening effect, especially in the alloys with Zr + Sc additions (doubling the hardness). $Al_3Zr$ and $Al_3(Zr,Sc)$ coherent particles are identified as hardening nanoprecipitates. The compressive mechanical testing at room and elevated temperatures shows that the additions of Zr and Zr + Sc improve the strength with the additional increase caused by ultrasonic melt processing.**

## 1. Introduction

Aluminum–cerium alloys represent one of the alternative materials that can find use in automotive applications where a combination of light weight, good casting properties, high thermal/electrical conductivity, and thermal stability is needed, for example, in next-generation automotive EV models.[1,2] Al–Ce-based alloys perform well at both room and elevated temperatures owing to the formation of thermally stable intermetallics.[1,3] Moreover, fine and thermally stable eutectic $Al_{11}Ce_3$ particles produce significant strengthening while preserving ductility.[1,4] There is a growing trend of using Al–Ce alloys in various applications. Binary Al–Ce alloys have demonstrated good casting properties[3] and ternary Al–4Ce–8Fe[5] and Al–4Ce–2Ni[6] alloys showed potential to be used at elevated temperature with superior strength and wear resistance as compared to traditional aluminum alloys.[1] When studying different types of ternary eutectic Al–Ce–x alloys, the Al–Ce–Ni system was shown to have a good combination of high mechanical properties at room and elevated temperatures along with very good casting properties.[6]

Although the eutectic structure of Al–Ce–Ni alloys is generally rather fine, when the compositions are hypoeutectic the aluminum dendrites need to be refined to assure defect-free sound castings and improved ductility and toughness.[6] Ultrasonic melt processing (USP) is one of the advanced and environment-friendly techniques to improve the structure of as-cast metallic materials,[7,8] especially those based on Al and Mg.[9,10] Primary $Al_3Zr$ particles were shown to play an important role upon USP providing efficient nucleation sites for the aluminum and eutectic grains.[11,12]

Precipitation (or dispersion) hardening treatment is an efficient way to improve high-temperature mechanical properties

S. Chankitmunkong
Department of Industrial Engineering
School of Engineering
King Mongkut's Institute of Technology Ladkrabang
Bangkok 10520, Thailand

F. Wang
School of Metallurgy and Materials
University of Birmingham
B15 2SE Birmingham, UK

The ORCID identification number(s) for the author(s) of this article can be found under https://doi.org/10.1002/adem.202301045.

**DOI: 10.1002/adem.202301045**

C. Limmaneevichitr
Department of Production Engineering
Faculty of Engineering
King Mongkut's University of Technology Thonburi
126 Pracha-Utid Road, Bangmod, Tungkhru, Bangkok 10140, Thailand

D. G. Eskin
Brunel Centre for Advanced Solidification Technology
Brunel University London
BCAST
Uxbridge UB8 3PH, Middlesex, UK
E-mail: dmitry.eskin@brunel.ac.uk

D. G. Eskin
Department of Mathematical Physics
Tomsk State University
634050 Tomsk, Russian Federation

through thermally stable nanoprecipitates formed typically by transition elements. Aluminum–scandium (Al–Sc) alloys show excellent mechanical properties at ambient and elevated temperature[13] due to the precipitation of numerous coherent, nanosized $Al_3Sc$ particles with the $L1_2$ crystal structure.[14] At elevated temperature, the $Al_3Sc$ precipitates have high thermal stability because of the low diffusivity of Sc in Al and low coarsening rate.[15] By substituting a portion of scandium (Sc) with zirconium (Zr) in the alloy, it is possible to achieve cost reduction without compromising alloy's desirable mechanical properties at both room temperature and elevated temperatures.[16] The thermal stability and working temperatures of Al–Sc alloys can be increased with addition of Zr (the hardening temperature increasing from 250 to 350–400 °C).[17] Sc-free Al–Zr alloys also have a potential for dispersion hardening though with a somewhat smaller hardening effect.[18] Recently it was demonstrated that the addition of Sc and Zr to binary Al–1.5Ce alloys resulted in significant hardening through the combination of micrometer-sized $Al_{11}Ce_3$ particles formed upon solidification and nanosized $Al_3$(Sc, Zr) precipitates.[19] It was also reported that additions of Zr and Sc refined primary $Al_{11}Ce_3$ particles in hypereutectic Al–Ce alloys through nucleation of $Al_3$(Zr, Sc) substrates.[20]

To the best of our knowledge, there was no previous study on the synergetic effects of USP for the structure refinement combined with dispersion hardening from $Al_3Zr$ ($Al_3$(Zr, Sc)) particles in the Al–Ce–Ni system. Such a study would have implications for improving the technological, mechanical and functional properties for wider applications in modern manufacturing, e.g., automotive engines and battery enclosures, automotive structural castings, aerospace products, etc.

Thus, this article is aimed at studying a combination of two mechanisms for the structure and properties control in a promising Al–Ce–Ni–Zr–Sc alloying system: 1) structure refinement by using USP and 2) dispersion hardening by precipitates formed during annealing. Alongside a thorough structure examination, we demonstrate an improvement of mechanical properties at room and elevated temperatures while preserving high electric/thermal conductivity.

## 2. Experimental Section

### 2.1. Alloy Preparation

The experimentally cast alloys of Al–4Ce–2Ni, Al–4Ce–2Ni–0.3Zr, and Al–4Ce–2Ni–0.15Zr–0.15Sc (all compositions were in wt%) were prepared from 99.9% pure Al, Al–20% Ce, Al–17% Ni, Al–2% Sc, and Al–10% Zr master alloys. The selection of the base composition was based on the previous work by Belov et al.[6] The solidification range of the experimental alloys was calculated using Thermo Calc software (version 2023a) with a Scheil model using the TCAL8 database. This was used in determining the temperature range for ultrasonic processing upon the formation of primary $Al_3$(Zr, Sc) phase in the alloy. The alloys were melted at 800 °C in SiC crucible in an electric furnace. The dross and oxide layer were skimmed before molten metal pouring. The alloy without ultrasonic processing was poured at 730 °C into a thick-walled cylindrical steel mold (90 mm outer diameter, 30 mm inner diameter, and 200 mm height), with an approximate solidification rate of $10°C\,s^{-1}$. USP was performed using a Reltec water-cooled magnetostrictive transducer with a driving frequency of 17.5 kHz at 3.5 kW (≈25 μm amplitude) equipped with the niobium sonotrode 20 mm in diameter. The sonotrode tip was preheated at 600 °C and then submerged into the melt. USP was performed in the temperature range from 780 to 730 °C before pouring into the same mold as earlier. The chemical composition of each alloy is given in **Table 1** as an average from three measurements by spark optical emission spectrometry (Foundry Master).

**Table 1.** Chemical compositions of the experimental alloys.

| Nominal composition [wt%] | Alloy | Experimental composition [wt%] | | | | |
|---|---|---|---|---|---|---|
| | | Ce | Ni | Zr | Sc | Al |
| Al–4Ce–2Ni | AlCeNi | 4.02 | 2.15 | – | – | Balance |
| Al–4Ce–2Ni | AlCeNi-USP | 4.04 | 2.17 | – | – | ” |
| Al–4Ce–2Ni–0.3Zr | AlCeNiZr | 4.01 | 2.13 | 0.3 | | ” |
| Al–4Ce–2Ni–0.3Zr | AlCeNiZr-USP | 4.05 | 2.13 | 0.3 | | ” |
| Al–4Ce–2Ni–0.15Zr–0.15Sc | AlCeNiZrSc | 4.02 | 2.16 | 0.15 | 0.15 | ” |
| Al–4Ce–2Ni–0.15Zr–0.15Sc | AlCeNiZrSc-USP | 4.04 | 2.15 | 0.15 | 0.15 | ” |

### 2.2. Microstructure Analysis

Samples for metallographic examination were cut from the center of the castings. The specimens were polished following standard metallographic procedures and the microstructures were observed in an optical microscope (OM, Zeiss Axio Scope.A1). The samples were also anodized in Barker's solution (5% $HBF_4$ water solution) for about 2 min at 20 VDC and were then examined in the OM under polarized light. The average grain sizes were measured by the linear intercept method according to ASTM E112-10. At least 30 measurements from different ten images were made on each specimen to the quantitative analysis.

The primary and eutectic phases were characterized by a field-emission scanning electron microscope (FESEM, Thermo Scientific Apreo S) equipped with an energy-dispersive spectroscopy (EDS) detector. In addition, X-Ray diffractometer (XRD, Bruker D8 advance) with a Cu Kα radiation source was used to determine the phase composition of the specimens.

To analyze the nanoprecipitates after the aging treatment at 350 °C for 30 h, the specimens were cut from the samples containing 0.3% Zr and 0.15% Zr + 0.15% Sc additions and ground to about 100 μm thickness. Then, 3 mm-diameter discs were punched from the foil specimens and further thinned to perforation by precision ion-polishing system (Gatan PIPS Model 691). The specimens were examined in a JEOL-2100F transmission electron microscope (TEM). Furthermore, the amount of Zr in the supersaturated Al matrix was measured with EDS in a ZEISS Supra 35 SEM.

### 2.3. Mechanical and Electrical Conductivity Testing

The specimens 25 mm in radius and 20 mm in thickness were cut from the castings. For dispersion hardening, the specimens were annealed at 350 °C and then quenched in water each 3 h in steps up to 30 h. The annealing temperature was selected following the previous studies.[21] Hardness test was conducted using a Brinell Innovatest hardness tester (Nexus 3200) with 625 N load, 2.5 mm ball indenter, and 20 s dwell time. At least ten measurements were made on each specimen.

For compressive testing, the specimens were machined from the central portions of the castings into cylindrical specimens 10 mm long and 5 mm in diameter. The samples were annealed at 350 °C for 30 h prior to testing. Compressive experiments were conducted in a quench-deformation dilatometer DIL 805 A $D^{-1}$. The as-cast and annealed (350 °C, 30 h) samples were compressed at 30 and 300 °C with a strain rate of 1 $s^{-1}$. A thermocouple was welded on the specimen to monitor the temperatures during testing. The specimen was initially fixed in the chamber between punches and then the force was applied from the initial length of 10–5 mm at 30 °C. For the high-temperature condition, the sample was set up in the chamber and then heated to 300 °C with a heating rate of 10 °C $s^{-1}$, held for 3 min, and subsequently compressed from the initial length of 10–5 mm at the same strain rate. Finally, it was quenched with argon gas flow. Compressive true stress–true strain curves were automatically recorded during the entire test cycle.

The electrical conductivity was measured on the surface specimens that were annealed at 350 °C for 30 h using Sigmatest 2.069 (Forester Instruments) at a frequency of 120 kHz.

## 3. Results and Discussion

### 3.1. Thermo-Calc Calculations for the Solidification Sequence

We intended to use the mechanism of structure refinement through USP that involved enhanced heterogeneous nucleation and fragmentation of primary $Al_3Zr$ particles due to ultrasonic

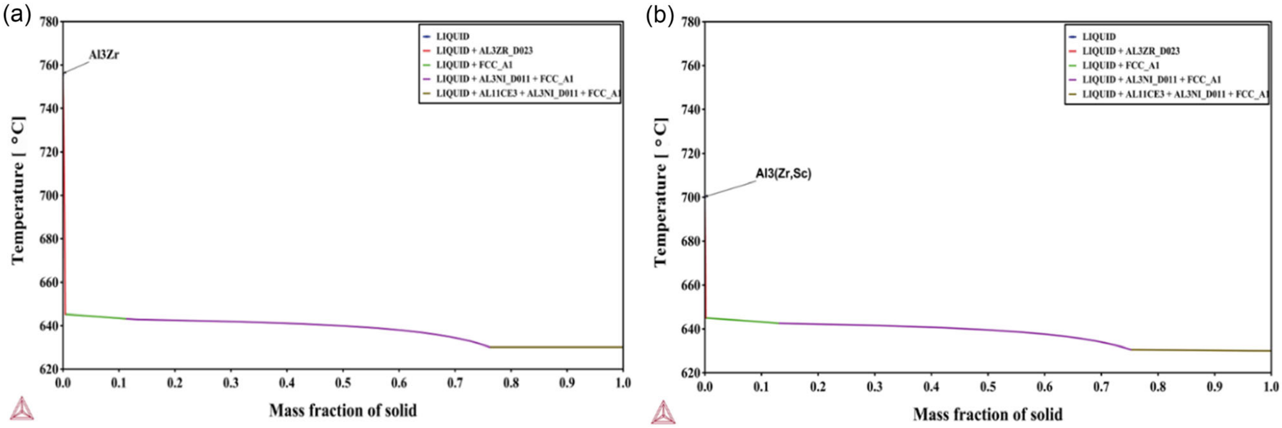

**Figure 1.** Scheil simulation for solidification of an Al–4Ce–2Ni alloy with: a) the addition of 0.3% Zr and b) the addition of 0.15% Sc and 0.15% Zr.

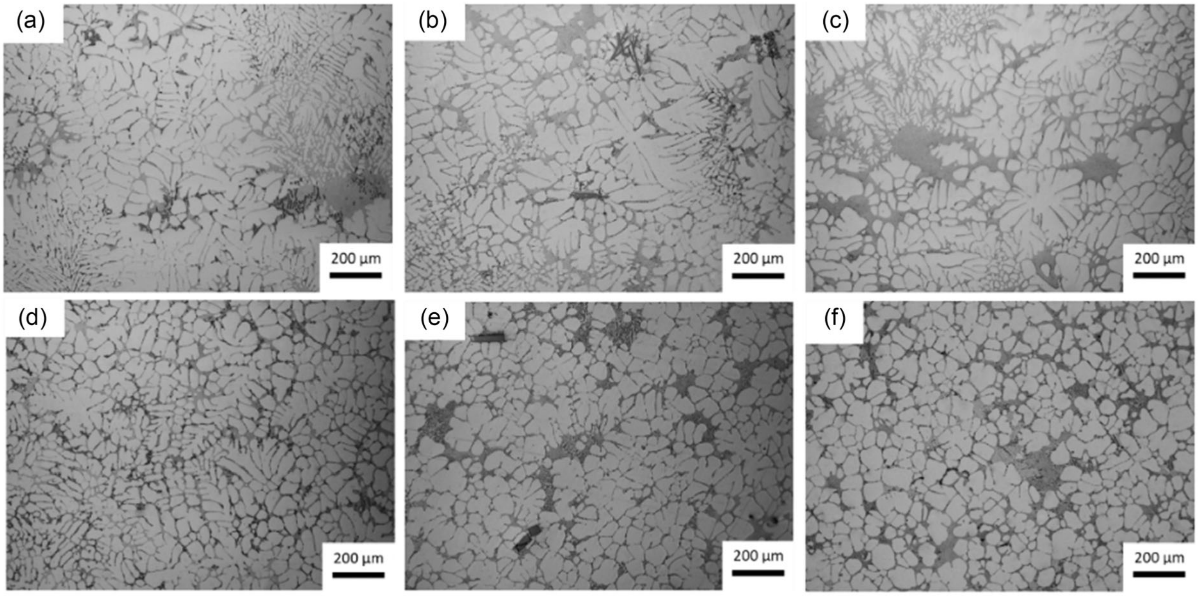

**Figure 2.** Optical macrographs of as-cast specimens, showing grain and eutectic structure, without USP: a) AlCeNi, b) AlCeNiZr, c) AlCeNiZrSc; with USP: d) AlCeNi-USP, e) AlCeNiZr-USP, f) AlCeNiZrSc-USP.

cavitation. In order to select the proper temperature range that will facilitate this mechanism, we calculated the sequence of phase formation in the Al–4Ce–2Ni alloy with Zr and Zr + Sc additions, as shown in **Figure 1**. The results showed that the addition of 0.3 wt% Zr to the base alloy resulted in the increase of liquidus temperature, with the formation of the $Al_3Zr$ primary phase at 755 °C, as shown in Figure 1a. When the amount of Zr decreased to 0.15 and 0.15 wt% Sc was added, the primary $Al_3(Zr, Sc)$ phase started to form at 700 °C, as shown in Figure 1b. Then the eutectic phases were formed in the range 645–630 °C. Therefore, the USP in the experiment was applied in the temperature range of 780–690 °C, that is, in the temperature range from the fully liquid state into the primary $Al_3Zr$ ($Al_3(Zr,Sc)$) phase formation range. According to our previous work, such a temperature range will result in the best results in terms of the primary phase refinement.[22] Note that the USP done at lower temperatures, for example, during the eutectic solidification, would typically result in the coarsening of the eutectic due to the acoustic energy introduced, which would slow down the eutectic solidification.[7]

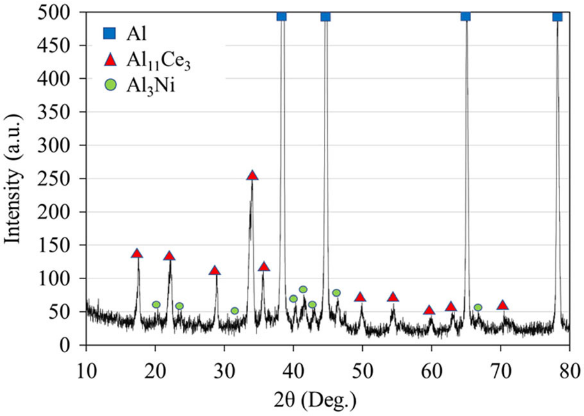

**Figure 3.** XRD patterns of the as-cast AlCeNi alloy.

### 3.2. Microstructure and Phase Analysis

The as-cast microstructures of the ternary AlCeNi alloy and the alloys with additions AlCeNiZr and AlCeNiZrSc alloys without USP are shown in **Figure 2**a–c and with USP in Figure 2d–f, respectively.

One can see that the structure consisted of Al dendrites and relatively large eutectic patches. The additions of Zr or Zr + Sc did not change much the grain structure in the alloys without USP. With the USP, the structure became more uniform, irrespective of the Zr (Sc) additions, while the dendrites were refined after USP with Zr and Zr + Sc additions, as shown in in Figure 4. One can notice primary $Al_3Zr$ particles in Figure 2b,e. The difference is that primary particles agglomerated in the alloys without USP while after USP they were fragmented and dispersed. The alloys with Zr and Sc did not show any large primary particles, most likely due to the much lower amount Zr.

The eutectic constituents in the alloys were confirmed to comprise $Al_{11}Ce_3$ ($Al_4Ce$) and $Al_3Ni$ phases in accordance with Thermo Calc calculations (Figure 1). **Figure 3** shows XRD spectra with the $Al_{11}Ce_3$ and $Al_3Ni$ phases agreeing with the Thermo Calc results in Figure 1.

**Figure 4** shows the grain structure in the tested alloys (optical micrographs in polarized light). These results confirmed that the addition of Zr or Zr + Sc to the base alloy did not change much the grain structure (Figure 2a–c and 4a–c), while the situation dramatically changed upon USP when the grain structure became significantly refined (**Figure 5**e), especially upon joint Zr and Sc additions (Figure 4f). These observations were further supported by the quantitative data in Figure 5, with the average

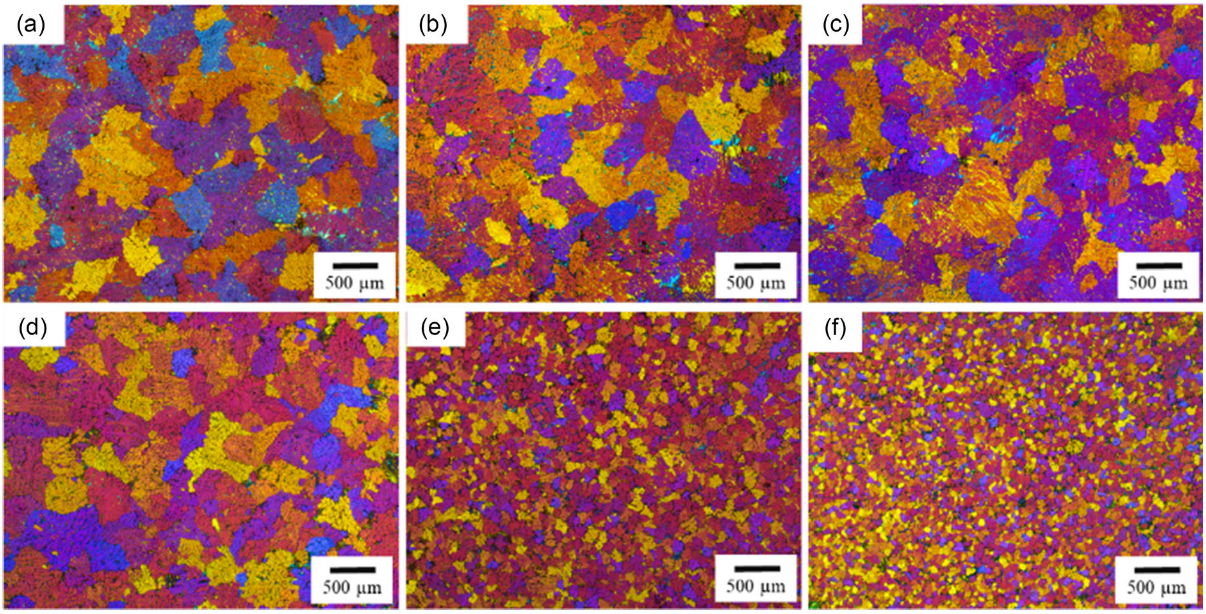

**Figure 4.** Optical polarized micrographs of the as-cast specimens, demonstrating grain structures: without USP: a) AlCeNi, b) AlCeNiZr, c) AlCeNiZrSc; with USP: d) AlCeNi-USP, e) AlCeNiZr-USP, f) AlCeNiZrSc-USP.

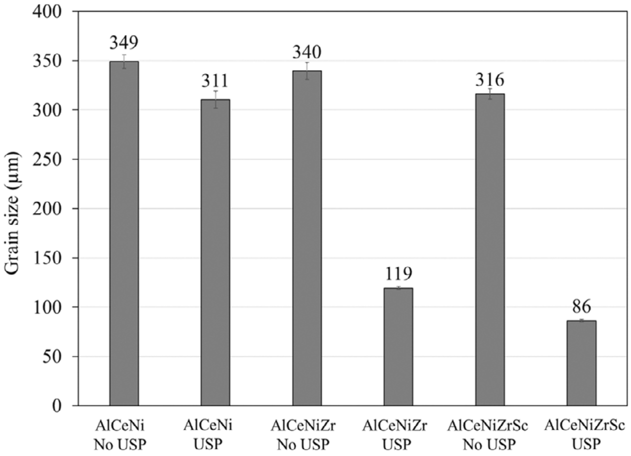

**Figure 5.** Grain size of the alloys with and without USP.

grain size decreasing from about 350 µm in the base alloy to ≈120 and 85 µm in the alloys with Zr and Zr + Sc additions subjected to USP. These results confirmed that the mechanisms of structure refinement induced by the presence of Zr and USP were successfully employed in the structure control of the tested Al–Ce–Ni alloys.

These mechanisms have been studied in detail elsewhere for other groups of Al alloys and include the heterogeneous nucleation of primary $Al_3Zr$ particles on the oxide inclusions activated by ultrasonic cavitation followed by the refinement through fragmentation of these particles by shock waves and acoustic flows induced by cavitation.[7,11,12,23]

**Figure 6** and **7** demonstrate the results of these mechanisms. One can see that the USP resulted in a significant refinement of primary $Al_3Zr$ in the alloy with 0.3% Zr (compare Figure 6a,b), while in the alloy with 0.15% Zr and 0.15% Sc no primary phase was found without USP but USP triggered the nucleation of this phase and then refined it (compare Figure 6c,d). It is well known that Zr and Sc tend to supersaturate aluminum solid solution upon solidification rather than form primary particles, which explains the absence of these particles in the alloy containing lesser amount of Zr and solidified without USP. Ultrasonic cavitation facilitates nucleation of primary phases on activated inclusions and therefore triggers the formation of the primary particles while also fragmenting them. Figure 7 presents the EDS mapping of some particles, confirming that they contain Zr and Sc. There was also some dissolved Ce (not shown here). The location of the particles inside the grains (Figure 6b,d, 7a) gives a clue to their role as nucleation substrates. It is interesting that Sc tends to form an outer layer on the $Al_3Zr$ particles (Figure 7i), which is similar to that already reported by us earlier.[24] This Sc-rich layer may improve the nucleating ability of the $Al_3Zr$ phase by changing the surface structure, making it close to $Al_3Sc$. The role of Ce in $Al_3Zr$ needs to be studied in more detail.

Therefore, the mechanisms of USP-induced structure refinement in aluminum alloys with Zr were demonstrated to work in the Al–Ce–Ni alloying system as well.

### 3.3. Dispersion Hardening and Electrical Conductivity

**Figure 8** shows the hardness of the as-cast alloys (a) as well as the hardening upon annealing at 350 °C (b). The hardness of the as-cast alloys did not change much with addition of Zr, Sc, or USP, with a slight tendency to increase in the alloys with Zr/Sc additions and decrease with USP in these alloys. The base alloy did not show any hardening effect upon annealing, while the alloys with 0.3% Zr demonstrated a moderate hardening effect

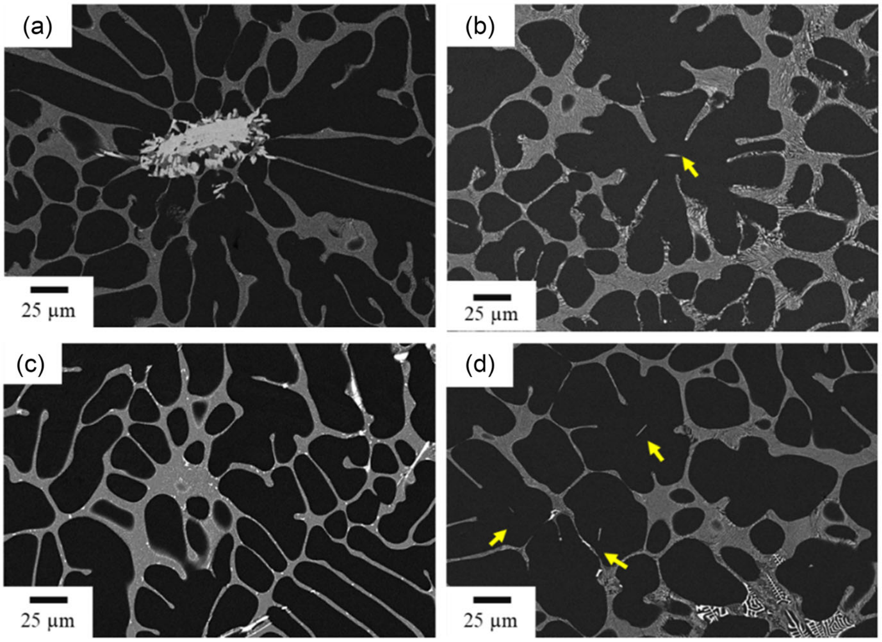

**Figure 6.** SEM images of primary $Al_3Zr$ particles: a) AlCeNiZr, b) AlCeNiZr-USP, c) AlCeNiZrSc, and d) AlCeNiZrSc-USP. Yellow arrows show the refined primary $Al_3Zr$ particles.

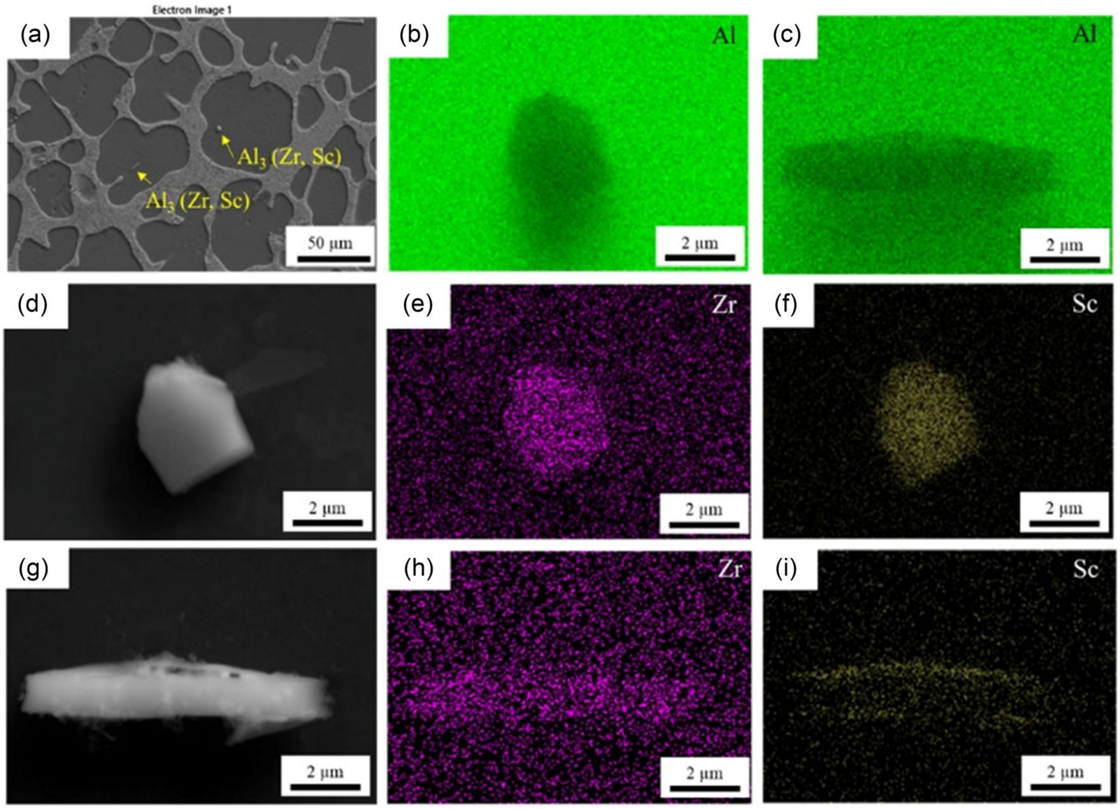

**Figure 7.** SEM images of primary particles a,d,g) in the AlCeNiZrSc-USP alloy; corresponding EDS mapping of b,c) Al, e,h) Zr, f,i) Sc.

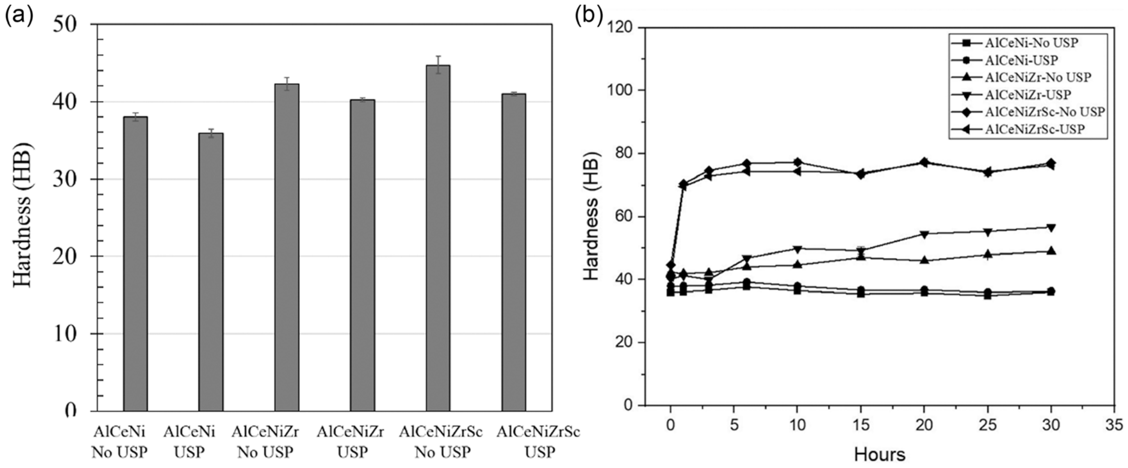

**Figure 8.** The hardness of a) as-cast alloys and b) the alloys annealed at 350 °C for up to 30 h.

(≈15 HB) and the alloys with 0.5% Zr and 0.15% Sc had a significant hardening effect (≈40 HB or doubling the initial hardness). As shown in Figure 8b, USP had a rather small effect on hardening, most noticeable in the alloys with 0.3% Zr. Note that the substantial grain refinement (Figure 4) was not reflected on the hardness or hardening effect.

The electrical conductivity measurements in **Figure 9** demonstrated that additions of Zr and Zr + Sc resulted in overall decrease of the conductivity that was somewhat restored upon annealing, especially in the alloys containing Zr + Sc. USP did not have any significant effect of this property. It is well known that the electrical (and thermal) conductivity depends on the amount of alloying elements in the supersaturated solid solution, stresses induced by coherent precipitates, and the overall presence of interfaces. Zr and Zr + Sc tend to supersaturate the aluminum solid solution upon solidification. Therefore, we see a substantial decrease in the conductivity of the as-cast alloys with the additions of Zr and Zr + Sc. Although USP triggered nucleation of the primary $Al_3Zr$ phase (which in principle should lead to the lesser amount of Zr available for supersaturation), we did not see any consequence of that for the conductivity. Therefore, we can assume that the amount of Zr in the solid solution was close to its limit of supersaturation at the given cooling rate. **Figure 10** gives the measurements of the Zr concentration retained in the solid solution after casting. It can be seen that the average concentration of retained Zr is between 0.15% and 0.18%, with USP only slightly affecting this, mostly through the formation of primary particles (larger particles formed with USP deplete the solid solution of Zr). Therefore, the amount of Zr in the solid solution will be similar in the alloys with 0.3% and 0.15% Zr, which explains the similar values of conductivity. Sc in the solid solution had apparently a smaller effect on the conductivity. After precipitation of $Al_3Zr$ or $Al_3(Zr, Sc)$ phases, the conductivity was restored. However, it remained smaller in the

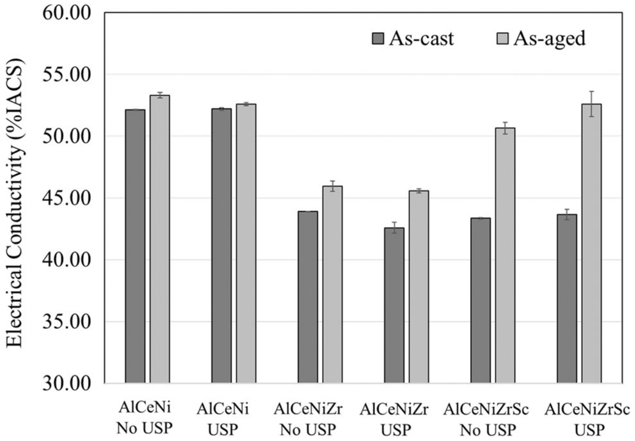

**Figure 9.** Electrical conductivity of the as-cast and annealed (350 °C, 30 h) alloys.

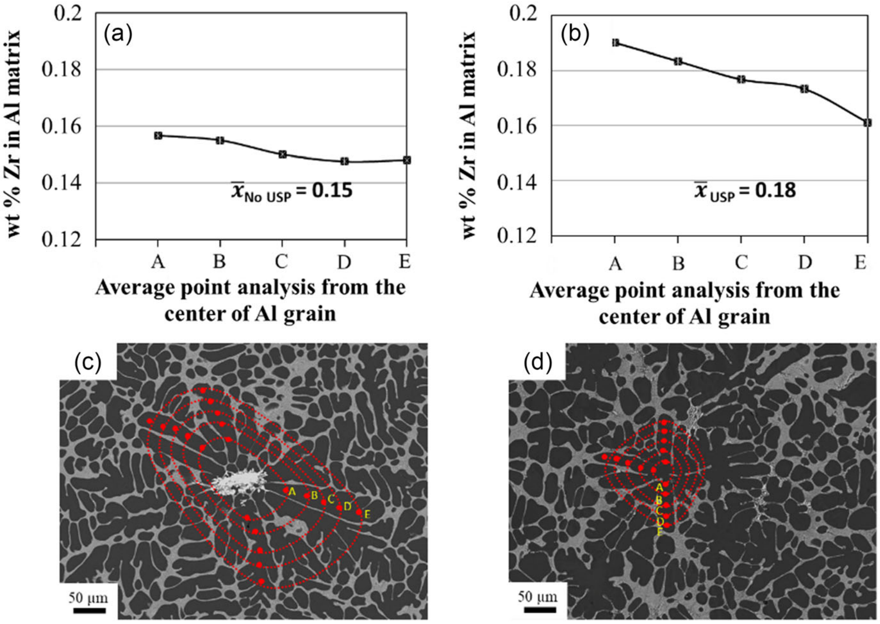

**Figure 10.** Measurements of Zr retained in the aluminum solid solution after solidification: a,c) AlCeNiZr and b,d) AlCeNiZr-USP. Error bars are smaller than the data point symbols.

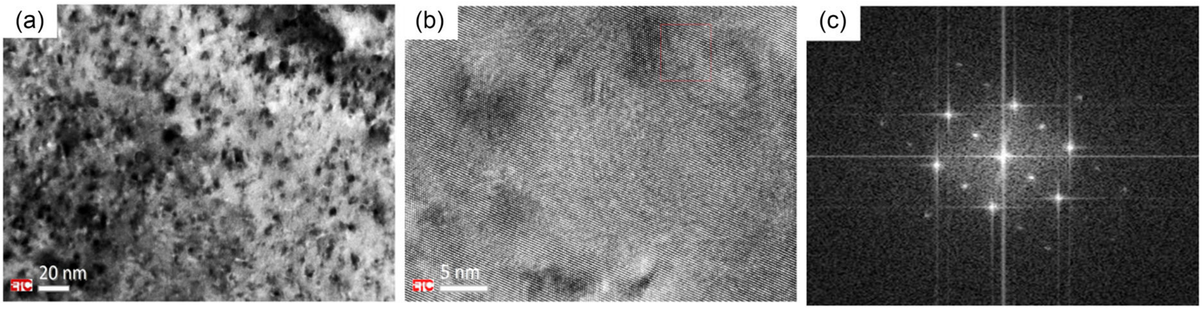

**Figure 11.** TEM images showing the $Al_3Zr$ precipitates in the annealed (350 °C, 30 h) AlCeNiZr alloy: a) morphology of $Al_3Zr$ precipitates distributed in Al matrix; b) high-resolution transmission electron microscopy (HRTEM) image of the $Al_3Zr$ precipitates, and c) the field-effect transistor (FET) related to b) confirming the presence of $L1_2$-type nanoprecipitates in this region.

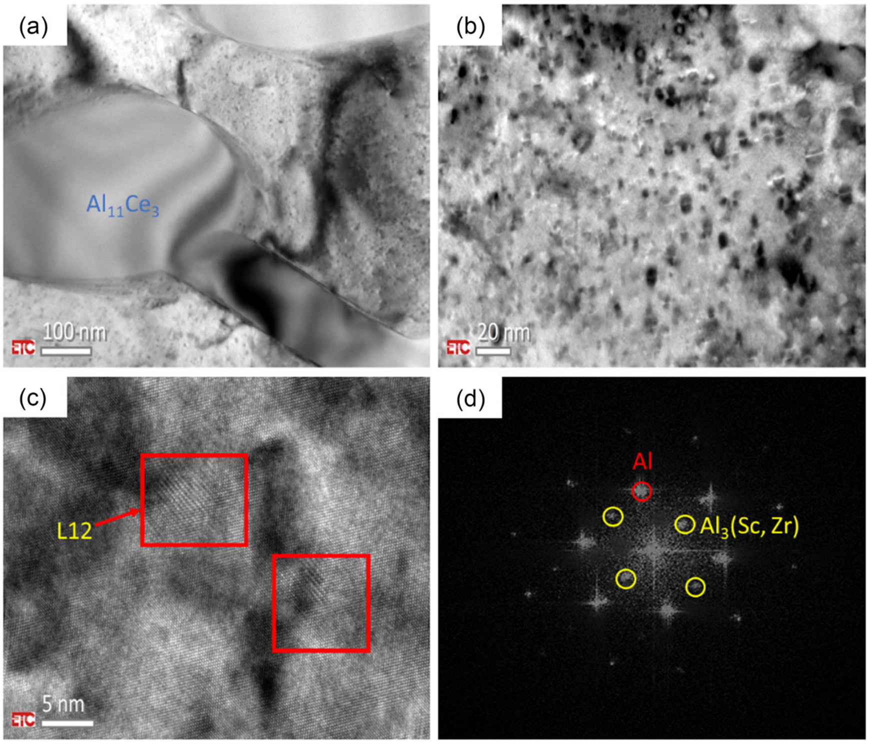

**Figure 12.** TEM images of annealed (350 °C, 30 h) AlCeNiZrSc alloy: a) the distribution of precipitates in the eutectic region, b) a higher magnification of $Al_3$(Zr, Sc) precipitates, c) HRTEM image showing $L1_2$ nanoprecipitates, and d) the FFT related to c) confirming the presence of $L1_2$-type nanoprecipitates in the marked area in (c).

AlCeNiZr alloys than in the AlCeNiZrSc alloys, which might be a consequence of the chosen annealing temperature. This temperature, that is, 350 °C, was sufficiently high for the complete precipitation of $Al_3$(Zr,Sc) phase while might be too low for the complete precipitation of $Al_3Zr$.[25] Although both these phases have a similar $L1_2$ structure and are coherent with the matrix, as demonstrated in **Figure 11** and **12**, the kinetics of their precipitation is different[13] with the $Al_3$(Zr, Sc) phase precipitating at a higher pace and having a core–shell structure (enriched Sc-core and Zr-rich shell) that is more efficient in hardening and slowing down the coarsening.[26,27]

### 3.4. Mechanical Properties at Room and Elevated Temperatures

Al–Ce–Ni alloys have the potential to be used in automotive and airspace applications as castings and, possibly, forgings. To assess the deformation behavior of these alloys at room and elevated temperatures, they were tested upon compression after being annealed at 350 °C for 30 h. The results are shown in **Figure 13** and **14**.

One can see that the additions of Zr and Zr + Sc consistently improved the yield stress and overall strength of the base alloy, for example, the Zr + Sc addition increased the room

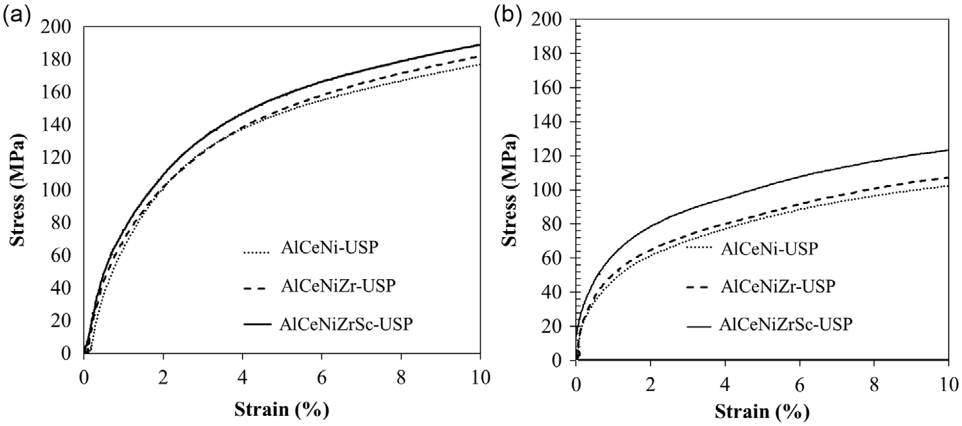

**Figure 13.** Compressive stress–strain curves of the dispersion-hardened alloys subjected to USP at two deformation temperatures: a) 30 °C and b) 300 °C.

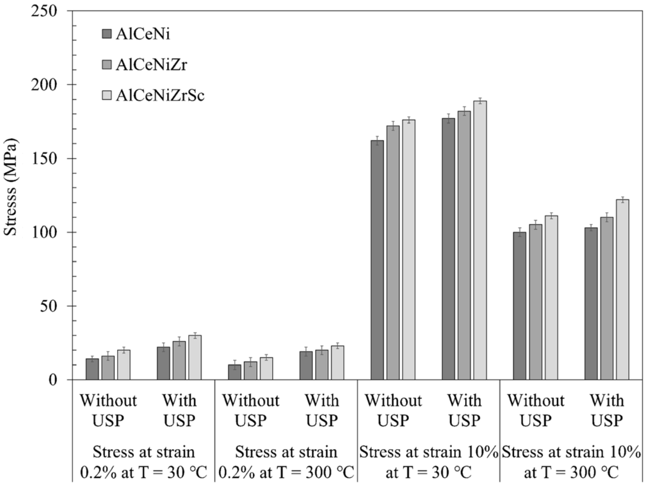

**Figure 14.** The 0.2% proof yield strength and the stress at 10% strain of the dispersion-hardened alloys tested at 30 and 300 °C.

temperature yield stress from 14 to 20 MPa and from 10 to 15 at 300 °C; and the compressive stress at 10% strain increased from 162 to 176 MPa at RT and from 100 to 111 MPa at 300 °C. USP gave an additional contribution to the compressive strength, reaching a yield stress of 30 MPa and a 10% stress of 189 MPa for the AlCeNiZrSc-USP alloy at room temperature. Similar improvements were for the samples tested at 300 °C.

The main reasons for the improvement of the compressive strength properties with Zr and Zr + Sc were the dispersion hardening induced by the $Al_3Zr$ and $Al_3(Zr, Sc)$ precipitates, as demonstrated in Section 3.3. As the annealing was done at the temperatures above the testing temperature, the hardening precipitates should remain relatively stable and the hardening effect should be preserved. Additional contribution from USP came from the grain refinement (see Figure 4 and 5). This grain refinement resulted in a more uniform distribution of intermetallics and ensured better deformability of the alloys with Zr and Zr + Sc, adding to the compressive strength.

## 4. Conclusion

The grain structure of hypoeutectic Al4Ce3Ni alloys can be significantly refined using the combination of Zr or Zr + Sc additions and USP in the temperature range of the primary $Al_3Zr$ intermetallic formation. The mechanisms known from the earlier studies involve the enhanced heterogeneous nucleation of $Al_3Zr$ on nonmetallic inclusions with subsequent refinement of the primary particles by fragmentation induced by ultrasonic cavitation. These refined particles then act as substrates for aluminum grains. Zr and Sc that supersaturate the aluminum solid solution upon solidification enable dispersion hardening upon annealing at 350 °C with either $Al_3Zr$ or $Al_3(Zr, Sc)$ precipitates, the latter offering a significantly better hardening response. There is a clear link between the hardening response and the concentration of Zr retained in the solid solution after solidification. The synergetic effect of both structure refinement upon solidification and the dispersion hardening upon annealing lead to the improved mechanical properties at room and elevated (300 °C) temperatures.

## Acknowledgements

The authors gratefully acknowledge FE-SEM Centre, School of Engineering, King Mongkut's Institute of Technology Ladkrabang, and financial support under project number RE-KRIS/FF66/29. D.E. acknowledges financial support from EPSRC (UK) under project grant PAAM (EP/W00593X/1). S.C. gratefully acknowledges BCAST (UK) for transmission electron microscopy facility support.

## Conflict of Interest

The authors declare no conflict of interest.

## Data Availability Statement

The data that support the findings of this study are available from the corresponding author upon reasonable request.

## Keywords

Al–Ce–Ni–Sc–Zr, aluminum alloys, electrical conductivity, nanocomposites, ultrasonic melt processing

Received: July 10, 2023
Revised: August 8, 2023

---

[1] Z. C. Sims, O. R. Rios, D. Weiss, P. E. Turchi, A. Perron, J. R. Lee, T. T. Li, J. A. Hammons, M. Bagge-Hansen, T. M. Willey, *Mater. Horiz.* **2017**, *4*, 1070.
[2] F. Czerwinski, *J. Mater. Sci.* **2020**, *55*, 24.
[3] Z. C. Sims, D. Weiss, S. K. McCall, M. A. McGuire, R. T. Ott, T. Geer, O. Rios, P. A. E. Turchi, *JOM* **2016**, *68*, 1940.
[4] D. Weiss, *J. Mater. Eng. Perform.* **2019**, *28*, 1903.
[5] Y.-H. Mashal, M. Kassem, A. Waheed, in *Stability, Wear, and Corrosion Characteristics of Rapidly Solidified High Temperature Al-8Fe-4Ce Alloy*, Tribology and Interface Engineering Series, Elsevier, Netherlands **2005**, pp. 703–708.
[6] N. A. Belov, E. A. Naumova, D. G. Eskin, *Mater. Sci. Eng. A* **1999**, *271*, 134.
[7] G. I. Eskin, D. G. Eskin, in *Ultrasonic Treatment of Light Alloy Melts*, CRC Press, London **2015**.
[8] S. Chankitmunkong, D. G. Eskin, C. Limmaneevichitr, *Mater. Sci. Eng. A* **2020**, *788*, 139567.
[9] A. P. Khrustalyov, A. A. Kozulin, I. A. Zhukov, M. G. Khmeleva, A. B. Vorozhtsov, D. Eskin, S. Chankitmunkong, V. V. Platov, S. V. Vasilyev, *Metals* **2019**, *9*, 1030.
[10] H. Kotadia, M. Qian, A. Das, *J. Alloys Compd.* **2020**, *823*, 153833.
[11] T. V. Atamanenko, D. G. Eskin, L. Zhang, L. Katgerman, *Metall. Mater. Trans. A* **2010**, *41*, 2056.
[12] D. Eskin, in *Ultrasonic Processing of Aluminium Alloys Above the Liquidus: The Role of Zr, MATEC Web of Conf.*, EDP Sciences, France **2020**, p. 06002.

[13] L. Toropova, D. Eskin, M. Kharakterova, T. Dobatkina, in *Advanced Aluminum Alloys Containing Scandium: Structure and Properties, Gordon an Breach OPA*, Routledge, London **1998**.

[14] E. A. Marquis, D. N. Seidman, *Acta Mater.* **2001**, *49*, 1909.

[15] S.-I. Fujikawa, in *Impurity Diffusion of Scandium in Aluminium*, Defect and Diffusion Forum, Trans Tech Publication, Netherlands **1997**, pp. 115–120.

[16] A. De Luca, D. C. Dunand, D. N. Seidman, in *Light Metals 2018* (Ed: O. Martin), Springer, Cham **2018**, pp. 1589–1594.

[17] C. B. Fuller, D. N. Seidman, D. C. Dunand, *Acta Mater.* **2003**, *51*, 4803.

[18] M. Song, Y. He, S. Fang, *J. Mater. Eng. Performance* **2011**, *20*, 377.

[19] C. N. Ekaputra, J. U. Rakhmonov, D. Weiss, J.-E. Mogonye, D. C. Dunand, *Acta Mater.* **2022**, *240*, 118354.

[20] J. Ye, K. Dai, Z. Wang, J. Chen, M. Gao, R. Guan, *Mater. Sci. Eng. A* **2022**, *835*, 142611.

[21] C. B. Fuller, D. N. Seidman, *Acta Mater.* **2005**, *53*, 5415.

[22] W. Feng, D. Eskin, T. Connolley, J.-W. Mi, *Trans. Nonferrous Met. Soc. China* **2017**, *27*, 977.

[23] A. Priyadarshi, M. Khavari, T. Subroto, M. Conte, P. Prentice, K. Pericleous, D. Eskin, J. Durodola, I. Tzanakis, *Ultrason. Sonochem.* **2021**, *70*, 105260.

[24] N. A. Belov, D. G. Eskin, A. A. Aksenov, in *Multicomponent Phase Diagrams: Applications for Commercial Aluminum Alloys*, Elsevier, Switzerland **2005**.

[25] N. Belov, A. Alabin, D. Eskin, V. Istomin-Kastrovskii, *J. Mater. Sci.* **2006**, *41*, 5890.

[26] C. B. Fuller, J. L. Murray, D. N. Seidman, *Acta Mater.* **2005**, *53*, 5401.

[27] E. Clouet, L. Laé, T. Épicier, W. Lefebvre, M. Nastar, A. Deschamps, *Nat. Mater.* **2006**, *5*, 482.